

Hidden covalent insulator and spin excitations in SrRu_2O_6

Diana Csontosová,^{1,2} Jiří Chaloupka,¹ Hiroshi Shinaoka,³ Atsushi Hariki,⁴ and Jan Kuneš^{1,2}

¹*Department of Condensed Matter Physics, Faculty of Science,
Masaryk University, Kotlářská 2, 611 37 Brno, Czechia*

²*Institute for Solid State Physics, TU Wien, 1040 Vienna, Austria*

³*Department of Physics, Saitama University, Saitama 338-8570, Japan*

⁴*Department of Physics and Electronics, Graduate School of Engineering,
Osaka Metropolitan University, 1-1 Gakuen-cho, Nakaku, Sakai, Osaka 599-8531, Japan*

(Dated: November 28, 2023)

The density functional plus dynamical mean-field theory is used to study the spin excitation spectra of SrRu_2O_6 . A good quantitative agreement with experimental spin excitation spectra is found. Depending on the size of the Hund's coupling J_H the systems chooses either Mott insulator or covalent insulator state when magnetic ordering is not allowed. We find that the nature of the paramagnetic state has negligible influence on the charge and spin excitation spectra. We find that antiferromagnetic correlations hide the covalent insulator state for realistic choices of the interaction parameters.

I. INTRODUCTION

Competition between kinetic and interaction energy is the corner stone of the correlated electrons physics. In the paradigmatic bandwidth control scenario of Hubbard model at half filling, increasing the interaction-to-bandwidth ratio suppresses the charge fluctuations and eventually drives the system to a Mott insulator (MI) state [1]. Real materials provide variations on this theme [2, 3], but also alternative mechanisms of correlation driven metal-insulator transition (MIT) such as site-selective Mott transition [4], spin-state crossover [5, 6], Kondo insulator [7], or gapping the ligand bands [8] to name a few. Often the paramagnetic (PM) MIT is hidden by a magnetic long-range order, which raises the question how much about the nature of the PM phase can be learned from the properties of the ordered phase. The studies of single-band Hubbard model [9, 10] found rather subtle differences in anti-ferromagnetic (AFM) phase on the two sides of the Mott transition, which can be difficult or even impossible to identify in multi-orbital setting of real materials.

A weakly correlated state does not have to be metallic in order to exhibit charge fluctuations. A covalent insulator (CI) [11], with a gap between bonding and anti-bonding states does as well. Mazin *et al.* [12] pointed out a special hopping pattern of t_{2g} electrons in layered transition metal oxides with honeycomb lattice and edge-sharing octahedra such as Na_2IrO_3 , $\alpha\text{-RuCl}_3$, Li_2RuO_3 or SrRu_2O_6 . Considering only the dominant hopping paths between the nearest-neighbor metal ions, the t_{2g} electrons are trapped on the hexagonal structural units, which gives rise to molecular orbitals clearly visible in the calculated non-interacting electronic spectra. At half filling the Fermi level falls into the band gap between the molecular peaks [13], which stabilizes the CI state. On the other hand, the tendency to form a high-spin MI is maximal also at half filling [14], which leads to a competition without an *a priori* winner.

This scenario is realized in SrRu_2O_6 with nominally

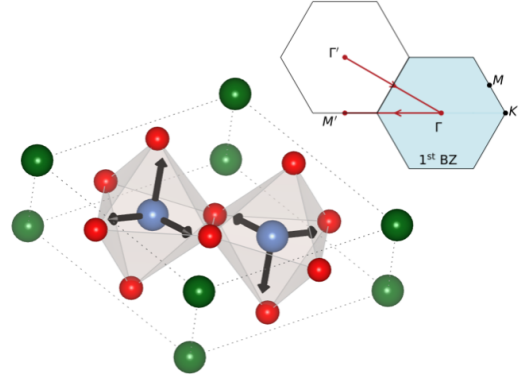


FIG. 1. The unit cell of SrRu_2O_6 : Ru (blue), O (red) and Sr (green) atoms, visualized using VESTA3 [15]. The arrows mark the local orbital coordinates. Path in the reciprocal space used for plotting magnon dispersions.

t_{2g}^3 configuration. An antiferromagnetic insulator with high Néel temperature T_N of 563 K [16], it does not exhibit the Curie-Weiss susceptibility in the PM phase. Instead, the susceptibility increases up to the highest reported temperature of about 730 K [17]. Classification of SrRu_2O_6 based on numerical studies has been controversial. Streltsov *et al.* [13] performed density functional plus dynamical mean-field theory (DFT+DMFT) calculations for Hund's coupling $J_H = 0.3$ eV. Pointing out the discrepancy between the theoretical ionic moment of $3 \mu_B$, a value essentially reproduced by their DFT+DMFT, and the observed ordered moment of $1.4 \mu_B$ they argued that the electronic structure of SrRu_2O_6 is dominated by molecular orbitals. Hariki *et al.* [18] using a similar DFT+DMFT approach found a crossover between CI and MI in the PM phase for J_H between $0.16 - 0.19$ eV, depending on temperature. They also found that in the AFM phase the size of the ordered moment is essentially the same on both sides of the CI/MI crossover and agrees well with experimental as well as the DFT value, when the overlaps of Wannier orbitals are properly accounted for. The uncertainty in

the value of the Hund's exchange J_H thus left the question of electronic structure of SrRu_2O_6 open.

Using resonant inelastic x-ray scattering (RIXS) to map out the magnon dispersion Suzuki *et al.* [19] concluded that SrRu_2O_6 is a Mott insulator because the magnon spectrum can be well described by $S = 3/2$ Heisenberg model with parameters obtained by strong-coupling expansion with first principles hopping parameters. They pointed out the difference between a large paramagnetic Néel temperature Θ , proportional to the inter-atomic exchange J and reflected in the magnon bandwidth, and the smaller ordering temperature T_N , determined by the spin gap. They argued that the observed absence of Curie-Weiss behavior above T_N is consistent with the behavior of 2D Heisenberg model, for which it is expected first for $T > \Theta$.

We compute the spin excitation spectra [20, 21] using DFT+DMFT [22]. We pursue two objectives (i) apply the DMFT approach to dynamical susceptibilities based of Bethe-Salpeter equation (BSE) [23, 24] to an ordered state of a real material and assess its quantitative accuracy, (ii) analyze the connection between the character of the PM phase, MI vs CI, and the properties of the AFM phase. The DMFT BSE approach has been successfully applied to antiferromagnetic magnons in up to 3-orbital model [24]. Here we focus on quantitative comparison with experiment, the role of spin-orbit coupling (SOC), the relationship between single-ion anisotropy and the spin gap, and other spin excitations beyond magnon. In order to address (ii), we vary J_H across the CI-MI crossover.

II. COMPUTATIONAL METHOD

We study the ' t_{2g} -only' model of Ref. 18 with Slater-Kanamori interaction obtained by wannierization [25, 26] from density functional calculation [27]. Unlike in Ref. 18 we use the basis of xy , yz and xz Wannier orbitals in the coordinates shown in Fig. 1, see Supplemental Material (SM) [28] and references [29–35] therein. In order to reduce the computational effort, the calculations were done for C-type (2 atoms) rather than the experimental G-type (4 atoms) structure. This approach is justified by the miniscule inter-layer coupling [17].

Several Ru compounds with honeycomb structure exhibit Ru-Ru dimerization upon cooling, Li_2RuO_3 [36], or under pressure, RuCl_3 [37] or $\text{Ag}_3\text{LiRu}_2\text{O}_6$ [38], which has been associated with a delicate balance between covalent bonding and spin-orbit entanglement [38]. Such behavior was observed neither in SrRu_2O_6 [17] nor in isoelectronic BaRu_2O_6 [39]. We speculate that this is related to the Ru d^3 configuration, which favors high-spin moment over spin-orbit entanglement (relative to other filling) and corresponds to one electron per each Ru-Ru bond. Therefore we perform our calculations for fixed experimental structure.

Throughout this study we keep the interaction param-

eter $U = 2.7$ eV fixed and vary $J_H = 0.16 - 0.22$ eV as well as temperature. In PM calculation we enforce the spin symmetry of the self-energy in each DMFT iteration.

The DMFT [40] calculations were performed with a multiorbital implementation [41] of the continuous-time hybridization expansion Monte Carlo method [42] based on ALPS core libraries [43]. Some of the DMFT calculations were benchmarked against results obtained with DCore [44]. The BSE with local particle-hole irreducible vertex [45] was solved for the lowest 10 bosonic Matsubara frequencies in the Legendre representation [46]. The desired dynamical susceptibilities $\langle O_{-\mathbf{q}} O_{\mathbf{q}} \rangle_{\omega}$ were obtained by sandwiching the general 2-particle susceptibility with the corresponding vertices followed by analytic continuation [47, 48], see SM [28] for details. The reciprocal space operators are related to local observable by the Fourier transform

$$O_{\mathbf{q}} = \sum_{\mathbf{R},s} e^{-i\mathbf{q}\cdot(\mathbf{R}+\mathbf{r}_s)} O_{\mathbf{R}s} \quad \mathbf{r}_s = \begin{cases} (\frac{2}{3}, \frac{1}{3}, 0) & s=A \\ (\frac{1}{3}, \frac{2}{3}, 0) & s=B, \end{cases} \quad (1)$$

where the index s refers to the two Ru sites in the unit cell. In the following we study the transverse spin susceptibility with $O \equiv S^x$, and $S = 3/2 \rightarrow 1/2$ excitations, for which we choose a representative operator $O \equiv X$ below, generating $\Delta S^z = \pm 1$ transitions between $S = 3/2$ and $S = 1/2$ manifolds

$$S_{\mathbf{R}s}^x = \sum_{\alpha=1}^3 d_{\mathbf{R}s\alpha\uparrow}^\dagger d_{\mathbf{R}s\alpha\downarrow} + H.c. \quad (2)$$

$$X_{\mathbf{R}s} = \left(d_{\mathbf{R}s1\uparrow}^\dagger d_{\mathbf{R}s1\downarrow} - d_{\mathbf{R}s2\uparrow}^\dagger d_{\mathbf{R}s2\downarrow} \right) + H.c. \quad (3)$$

The operator X is chosen to be representative of a set of closely spaced transitions, see SM [28].

III. RESULTS AND DISCUSSION

A. Magnon dispersion

The DMFT calculations lead to AFM with out of plane orientation of the local moment for temperatures below 1500 K. Since the magnetism of SrRu_2O_6 is essentially 2D [17, 19] this overestimation by DMFT is expected. The DMFT does not obey the Mermin-Wagner theorem and the calculated ordering temperature represents Θ rather than T_N . This does not mean that the DMFT AFM solution should not be able to capture the ordered state of the real material. Fig. 2 shows a comparison of the dynamical susceptibilities $\langle X_{-\mathbf{q}} X_{\mathbf{q}} \rangle_{\omega}$ and $\langle S_{-\mathbf{q}}^x S_{\mathbf{q}}^x \rangle_{\omega}$ calculated in the AFM phase at 464 K to the experimental RIXS data [19]. The magnetic moments at this temperature are essentially saturated [18, 28] and thus no significant change in the computed spectra is expected upon further cooling. Rather than computing the full RIXS spectra, calculation of which would require evaluation of transition amplitudes [49, 50] with the possibility

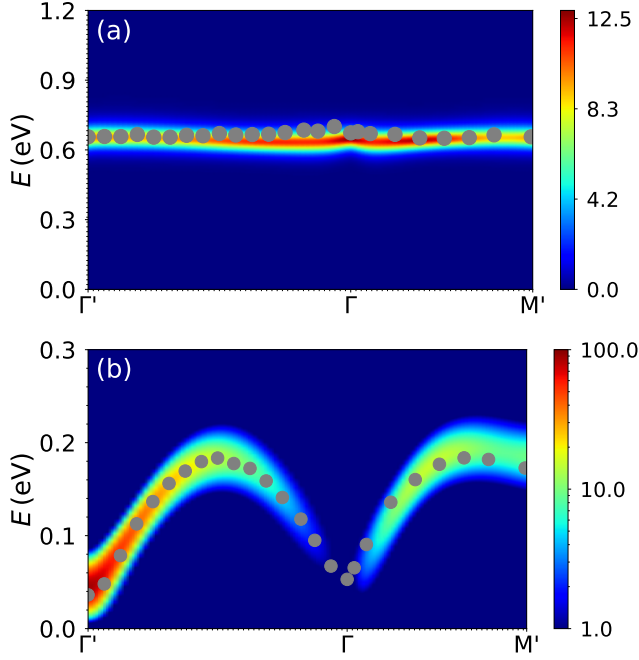


FIG. 2. Imaginary part of the dynamical susceptibility along the $\Gamma' - \Gamma - M'$ path shown in Fig. 1 for $J_H = 0.16$ eV at $T = 464$ K. Grey dots denote the maxima of the corresponding RIXS features [19]. Top (linear color scale): $\langle X_{-\mathbf{q}} X_{\mathbf{q}} \rangle_{\omega}$ representing the $S = 3/2 \rightarrow 1/2$ transitions. Bottom (logarithmic color scale): $\langle S_{-\mathbf{q}}^x S_{\mathbf{q}}^x \rangle_{\omega}$ corresponding to magnon.

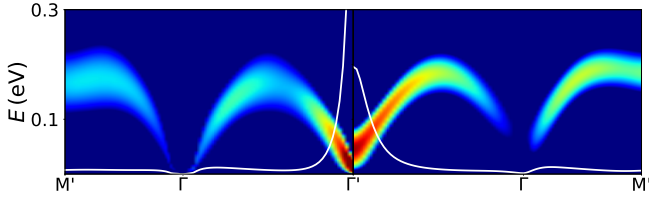


FIG. 3. Effect of the spin-orbit coupling (SOC) on the magnon spectra: with SOC (right panel) and without SOC (left panel). Color scale is the same as in Fig. 2b) The white line is a spectral weight computed as $\Omega_{\mathbf{q}} = -\frac{1}{\pi} \int_0^{0.3} d\omega \text{Im} \langle S_{-\mathbf{q}}^x S_{\mathbf{q}}^x \rangle_{\omega}$. The results were obtained for $J_H = 0.16$ eV and $T = 464$ K.

of multi-particle excitations [51, 52] and is not possible with the present methods, we compare the dispersions of specific spectral features. We find a very good match of the magnon dispersion including the bandwidth, the spin gap and the distribution of spectral weight. The magnon bandwidth of 183 meV corresponds to the effective nearest-neighbor exchange $JS = 61$ meV between $S = 3/2$ local moments.

A straightforward strong-coupling calculation with the same parameter setup yields a remarkably similar value $JS \approx 66$ meV [28], essentially unaffected by SOC. However, by inspecting the exact solution of our Hubbard model on a single bond [28], we found the spin $S = 3/2$ picture to be significantly disturbed by a large involvement of higher multiplet states at energies $\gtrsim 3J_H$ [28]. In

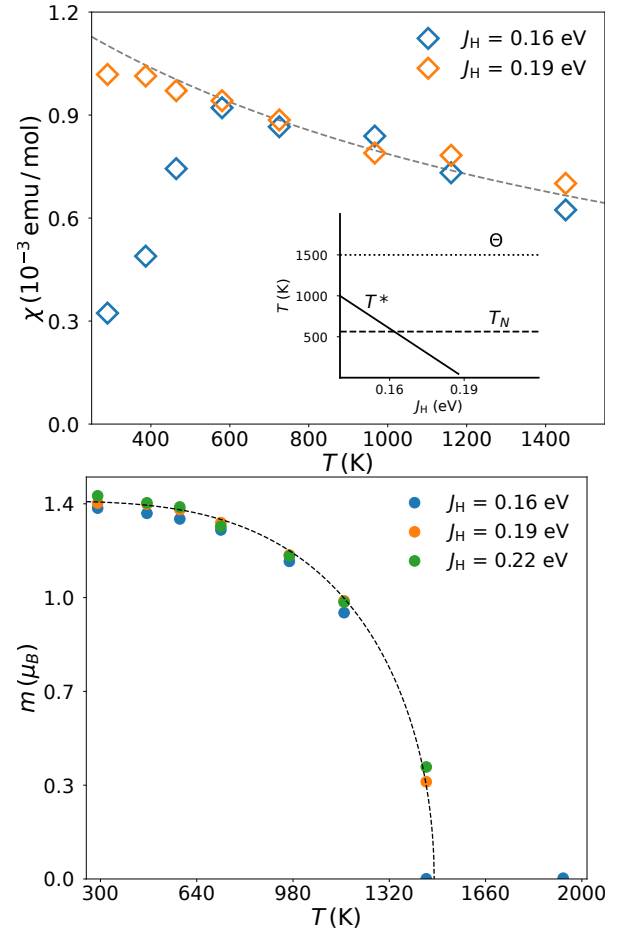


FIG. 4. Top panel: Uniform susceptibility for $J_H = 0.16$ eV and $J_H = 0.19$ eV in the PM state. The dashed line shows the Curie-Weiss susceptibility $\chi \propto (T + \Theta)^{-1}$ with $\Theta = 1480$ K. Magnitude of the calculated $\chi(T)$ is about 30% smaller than the experimental one [17]. Inset: a cartoon picture of different temperature scales in SrRu_2O_6 . Bottom panel: Order moment as a function of temperature for the studied values of J_H .

such situation, the DMFT approach covering the entire spectrum of multiplet states is highly advantageous.

The spin gap of approximately 45 meV is related to the single-ion anisotropy $\Delta_{\text{SIA}} = E_{\pm 1/2} - E_{\pm 3/2} = 6.6$ meV, defined as the difference between the atomic states belonging to the $S = 3/2$ multiplet [53]. The strong-coupling evaluation of SIA suggests that the above ionic value is actually strongly renormalized by exchange processes [28]. Within the linear spin-wave theory of Heisenberg antiferromagnet, the large gap is easily explained even for small SIA, as it is given by $S\sqrt{6J\Delta_{\text{SIA}}}$ [19]. Nevertheless, it is not self-evident that the present numerical approach must capture it accurately.

We have also carefully checked the out-of-plane orientation of the ordered moments, see SM [28], and verified its origin in SOC by performing calculations with $\text{SU}(2)$ -symmetric Hamiltonian without SOC. As expected we find two gapless linear Goldstone modes with divergent spectral weights in this case, see Fig. 3.

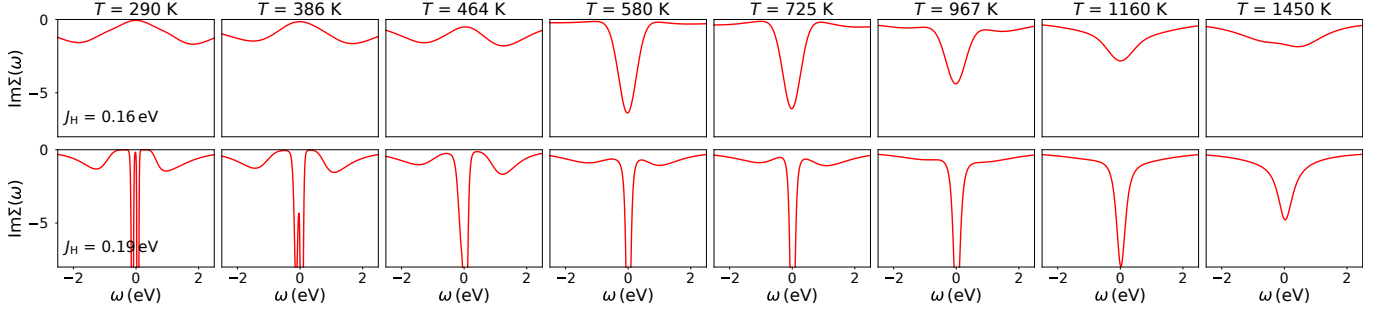


FIG. 5. Imaginary part of self-energy $\text{Im}\Sigma_{ii}(\omega)$ (diagonal element) on the real frequency axis for $J_H = 0.16$ eV (top row) and $J_H = 0.19$ eV (bottom row) at various temperatures T . The crossover temperature T^* for $J_H = 0.16$ eV lies between 464 K and 580 K.

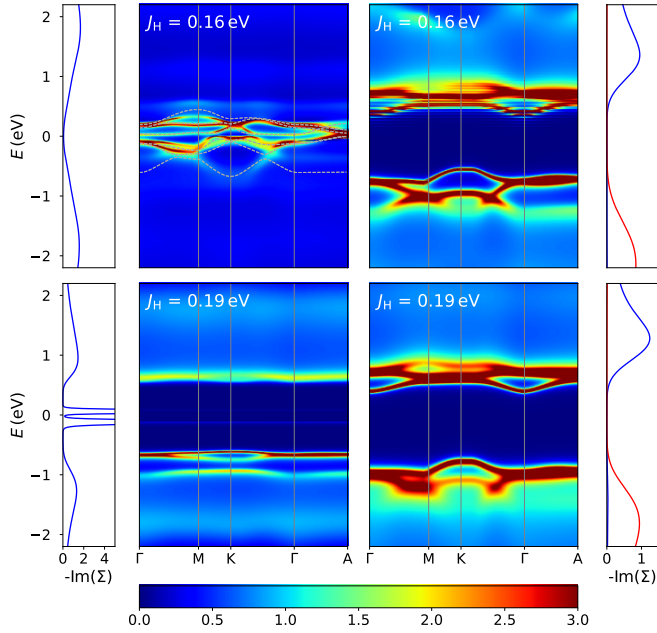


FIG. 6. Spectral functions and corresponding imaginary parts of self-energies on the real axis in the constrained PM solution (left half) and AFM solution (right half). The calculations were performed for $T = 290$ K. Red and blue color in the figures with AFM self-energies distinguish between spin up and spin down component. The grey lines in the spectral function with $J_H = 0.16$ eV show DFT band structure squeezed by factor 2.2.

The experimental RIXS spectra [19] exhibit a prominent low-energy feature associated with $S = 3/2 \rightarrow 1/2$ transitions. Our calculations, Fig. 2, reproduce the position of this feature fairly well, although the SOC induced mixing with the low energy magnon limits the resolution of the higher energy structures.

B. Mott vs covalent insulator

In calculations performed in the PM state, the authors of Ref. 18 observed a crossover between the low-temperature CI and high temperature MI at a scale T^* , which strongly depends on J_H . For $J_H = 0.16$ eV the scale T^* lies in the 600–800 K range, while for $J_H \gtrsim 0.19$ eV only MI was observed. SrRu_2O_6 exists in the PM phase below 800 K, however, since DMFT exaggerates its ordering temperature [54], we enforce the PM solution by constraint, in order to study it at lower temperatures.

The different temperature scales discussed below are summarized in the inset of Fig. 4. The paramagnetic Néel temperature Θ , which we identify with the DMFT ordering temperature, is estimated from the present study, the bottom panel of Fig. 4, and Ref. 18. The CI/MI crossover temperature T^* is estimated from Ref. 18 and the uniform susceptibility from $J_H = 0.16$ eV of this study. Finally, T_N is the experimental ordering temperature, the weak J_H -dependence of which may deduced from the behavior of the spin gap as a function of J_H .

Next, we discuss the properties of the constraint PM solutions. At high temperatures ($T > T^*$) CI and MI behave similarly. The imaginary part of the self-energy, shown in Fig. 5, exhibits a broad peak at the chemical potential, which give rise to a gap containing some incoherent spectral weight. At low temperatures ($T < T^*$) CI and MI are distinguished by several characteristics. The self-energy of CI has a Fermi liquid character with vanishing imaginary part at the chemical potential. The peak in MI self-energy becomes sharper and its background vanishes in the low-energy region, which defines the Mott gap. This gives rise to distinct band structures shown in Fig. 6. For the evolution of the self-energy on the imaginary axis see SM [28]. The CI and MI respond differently to a magnetic field. The magnetic susceptibility $\chi(T)$ of MI, in Fig. 4, exhibits the usual Curie–Weiss decrease with increasing temperature. The high-temperature susceptibility of CI follows the same trend. However, once the Fermi liquid behavior sets in below T^* [55] the susceptibility starts to drop, which gives rise

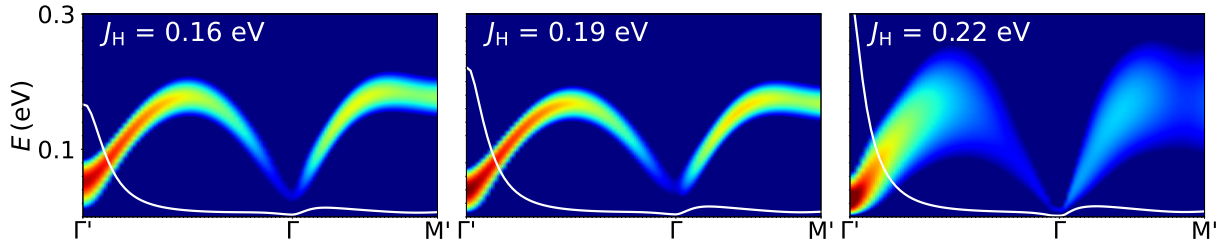


FIG. 7. Comparison of magnon spectra in covalent insulator ($J_H = 0.16$ eV) and Mott insulator ($J_H = 0.19$ eV and $J_H = 0.22$ eV) phases. The calculations were performed for $T = 464$ K. The spin gaps for $J_H = \{0.16, 0.19, 0.22\}$ eV are $\Delta_m = \{45, 36, 35\}$ meV, respectively. The white line is a spectral weight Ω_q . (The same color scale as Fig. 2b)

to a broad maximum. A positive slope of the experimental $\chi(T)$ above the transition temperature was pointed out by the authors of Ref. 17. The CI and MI states are also distinguished by local charge fluctuations on the Ru site [18]. This is reminiscent of the site selective Mott transition [4], where both CI- and MI-like sites are found within the same compound. Numerical simulations of core-level spectroscopies such as x-ray absorption or RIXS [56] revealed distinct dependencies on the incoming photon frequency. Similar spectroscopic signature may be expected for the CI and MI states.

How is the different character of the PM phase reflected in the AFM phase? Upon magnetic ordering the self-energy is dominated by the spin-dependent Hartree shift and electronic spectra for large and small J_H in Fig 6 resemble one another. In Fig. 7 we compare the magnon spectra obtained at 464 K for J_H values on both sides of CI/MI crossover. A difference is hardly noticeable. There is a discernible trend of decreasing spin gap with J_H , which follows from the behavior of the single-ion anisotropy. Overall the parameters extracted using strong-coupling theory describe the magnons equally well on CI and MI side in the parameter space.

Can the behavior of the CI susceptibility explain the experimentally observed behavior of $\chi(T)$ in the PM phase? Is it plausible that an improved theory, which pushes the calculated T_N to its experimental value below T^* , uncovers the CI susceptibility? We argue that it is not. The problem of DMFT description is not quantitative overestimation of T_N because of inaccurate treatment of the 3D aspect (inter-layer coupling) of the material. In fact the estimated inter-layer coupling [17] was shown to be by far too small to account for the observed T_N [19]. The problem is a conceptual inefficacy to distinguish between the paramagnetic Néel temperature Θ and the ordering temperature T_N . In fact the Θ given by DFT+DMFT, i.e., the onset of strong AFM correlations, is likely correct as suggested by the correct magnon bandwidth obtained in the calculation. DMFT does not exaggerate the onset temperature of the AFM correlations, but describes them as static (AFM order), while in the 2D reality they remain dynamical down to much lower temperature T_N determined by a spin gap. Although the spin gap itself is well captured, its effect on T_N is completely missing in the theory. The CI physics

can be realized if the crossover temperature T^* is above the onset of AFM correlations Θ . In the present case for smaller J_H we get $T_N < T^* < \Theta$ and thus the increase of $\chi(T)$ above T_N represents the physics of 2D Heisenberg magnet rather than that of CI.

We would like to point out the analogy of the present physics with the Kondo lattice model [57]. In both cases a local moment disappears below a certain temperature, T^* in CI or Kondo temperature in case of the Kondo lattice, if not correlated to other moments on the lattice. In both cases, inter-site correlations between the local moments can preclude their disappearance if sufficiently strong, which we conjecture to mean $T^* < \Theta$ in the present case. These are examples of a situation when inter-site interaction between the local excited states (carrying the local moments), eliminates the (non-magnetic) local ground states from the set of global low-energy states.

IV. CONCLUSIONS

We have calculated the spin excitation spectra of SrRu_2O_6 using DFT+DMFT approach and found a quantitative match with the experimental observations [19], notably for the spin gap due to the spin-orbit coupling. The paramagnetic state of SrRu_2O_6 , depending on the strength of the Hund's coupling J_H , exhibits either covalent insulator or Mott insulator characteristics below $T^* \approx 580$ K. Once in the AFM ordered state the magnon and electron excitation spectra are essentially the same for J_H on both sides of the covalent insulator / Mott insulator crossover. Our calculations for realistic J_H on both sides of the CI/MI crossover lead to the conclusion that T^* is substantially below the temperature Θ at which the AFM correlations set in and therefore the covalent insulator state remains always 'hidden'.

ACKNOWLEDGMENTS

The authors thank H. Suzuki for providing the experimental data of Fig. 2, A. Kauch for critical reading of the manuscript, and K.-H. Ahn for valued discussions in the early stage of this work. This work has received funding from QUAST-FOR5249 project I 5868-N (D.C., J.K.) of

the Austrian Science Fund (FWF), Czech Science Foundation (GAČR) project No. GA22-28797S (D.C., J.C.), JSPS KAKENHI Grant Numbers 21K13884, 23K03324 (A.H.), 21H01003, 23H03816, 23H03817 (H.S., A.H.), Austrian Federal Ministry of Science, Research and Economy through the Vienna Scientific Cluster (VSC) Re-

search Center and by the Ministry of Education, Youth and Sports of the Czech Republic through the e-INFRA CZ (ID:90254). H.S was supported by JSPS KAKENHI Grant Number 21H01041. H. S. thanks the Supercomputer Center, the Institute for Solid State Physics, and the University of Tokyo for the use of their facilities.

-
- [1] W. F. Brinkman and T. M. Rice, Application of gutzwiller's variational method to the metal-insulator transition, *Phys. Rev. B* **2**, 4302 (1970).
 - [2] E. Pavarini, S. Biermann, A. Poteryaev, A. I. Lichtenstein, A. Georges, and O. K. Andersen, Mott transition and suppression of orbital fluctuations in orthorhombic $3d^1$ perovskites, *Phys. Rev. Lett.* **92**, 176403 (2004).
 - [3] B. J. Kim, H. Jin, S. J. Moon, J.-Y. Kim, B.-G. Park, C. S. Leem, J. Yu, T. W. Noh, C. Kim, S.-J. Oh, J.-H. Park, V. Durairaj, G. Cao, and E. Rotenberg, Novel $J_{\text{eff}} = 1/2$ Mott state induced by relativistic spin-orbit coupling in Sr_2IrO_4 , *Phys. Rev. Lett.* **101**, 076402 (2008).
 - [4] H. Park, A. J. Millis, and C. A. Marianetti, Site-selective Mott transition in rare-earth-element nickelates, *Phys. Rev. Lett.* **109**, 156402 (2012).
 - [5] J. R. Patterson, C. M. Aracne, D. D. Jackson, V. Malba, S. T. Weir, P. A. Baker, and Y. K. Vohra, Pressure-induced metallization of the Mott insulator MnO , *Phys. Rev. B* **69**, 220101 (2004).
 - [6] J. Kuneš, A. V. Lukoyanov, V. I. Anisimov, R. T. Scalettar, and W. E. Pickett, Collapse of magnetic moment drives the Mott transition in MnO , *Nat. Mater* **7**, 198 (2008).
 - [7] Z. Fisk, J. Sarrao, S. Cooper, P. Nyhus, G. Boebinger, A. Passner, and P. Canfield, Kondo insulators, *Physica B Condens. Matter* **223-224**, 409 (1996), proceedings of the International Conference on Strongly Correlated Electron Systems.
 - [8] J. Kuneš, L. Baldassarre, B. Schächner, K. Rabia, C. A. Kuntscher, D. M. Korotin, V. I. Anisimov, J. A. McLeod, E. Z. Kurmaev, and A. Moewes, Metal-insulator transition in $\text{NiS}_{2-x}\text{Se}_x$, *Phys. Rev. B* **81**, 035122 (2010).
 - [9] G. Sangiovanni, A. Toschi, E. Koch, K. Held, M. Capone, C. Castellani, O. Gunnarsson, S.-K. Mo, J. W. Allen, H.-D. Kim, A. Sekiyama, A. Yamasaki, S. Suga, and P. Metcalf, Static versus dynamical mean-field theory of Mott antiferromagnets, *Phys. Rev. B* **73**, 205121 (2006).
 - [10] L. Fratino, P. Sémon, M. Charlebois, G. Sordi, and A.-M. S. Tremblay, Signatures of the Mott transition in the antiferromagnetic state of the two-dimensional hubbard model, *Phys. Rev. B* **95**, 235109 (2017).
 - [11] C. Fu and S. Doniach, Model for a strongly correlated insulator: FeSi , *Phys. Rev. B* **51**, 17439 (1995); J. Kuneš and V. I. Anisimov, Temperature-dependent correlations in covalent insulators: Dynamical mean-field approximation, *Phys. Rev. B* **78**, 033109 (2008); M. Sentef, J. Kuneš, P. Werner, and A. P. Kampf, Correlations in a band insulator, *Phys. Rev. B* **80**, 155116 (2009).
 - [12] I. I. Mazin, H. O. Jeschke, K. Foyevtsova, R. Valentí, and D. I. Khomskii, Na_2IrO_3 as a molecular orbital crystal, *Phys. Rev. Lett.* **109**, 197201 (2012).
 - [13] S. Streltsov, I. I. Mazin, and K. Foyevtsova, Localized itinerant electrons and unique magnetic properties of SrRu_2O_6 , *Phys. Rev. B* **92**, 134408 (2015).
 - [14] A. Georges, L. d. Medici, and J. Mravlje, Strong correlations from hund's coupling, *Annu. Rev. Condens. Matter Phys.* **4**, 137 (2013).
 - [15] K. Momma and F. Izumi, *VESTA3* for three-dimensional visualization of crystal, volumetric and morphology data, *J. Appl. Crystallograph.* **44**, 1272 (2011).
 - [16] C. I. Hiley, M. R. Lees, J. M. Fisher, D. Thompsett, S. Agrestini, R. I. Smith, and R. I. Walton, Ruthenium(v) oxides from low-temperature hydrothermal synthesis, *Angew. Chem. Int. Ed.* **53**, 4423 (2014).
 - [17] C. I. Hiley, D. O. Scanlon, A. A. Sokol, S. M. Woodley, A. M. Ganose, S. Sangiao, J. M. De Teresa, P. Manuel, D. D. Khalyavin, M. Walker, M. R. Lees, and R. I. Walton, Antiferromagnetism at $T = 500 > \text{K}$ in the layered hexagonal ruthenate SrRu_2O_6 , *Phys. Rev. B* **92**, 104413 (2015).
 - [18] A. Hariki, A. Hausoel, G. Sangiovanni, and J. Kuneš, Dft+dmft study on soft moment magnetism and covalent bonding in SrRu_2O_6 , *Phys. Rev. B* **96**, 155135 (2017).
 - [19] H. Suzuki, H. Gretarsson, H. Ishikawa, K. Ueda, Z. Yang, H. Liu, H. Kim, D. Kuskusta, A. Yaresko, M. Minola, J. A. Sears, S. Francoual, H.-C. Wille, J. Nuss, H. Takagi, B. J. Kim, G. Khaliullin, H. Yavaş, and B. Keimer, Spin waves and spin-state transitions in a ruthenate high-temperature antiferromagnet, *Nat. Mater* **18**, 563 (2019).
 - [20] H. Park, K. Haule, and G. Kotliar, Magnetic excitation spectra in BaFe_2As_2 : A two-particle approach within a combination of the density functional theory and the dynamical mean-field theory method, *Phys. Rev. Lett.* **107**, 137007 (2011).
 - [21] L. Boehnke and F. Lechermann, Getting back to NaCoO_2 : Spectral and thermoelectric properties, *physica status solidi (a)* **211**, 1267 (2013).
 - [22] G. Kotliar, S. Y. Savrasov, K. Haule, V. S. Oudovenko, O. Parcollet, and C. A. Marianetti, Electronic structure calculations with dynamical mean-field theory, *Rev. Mod. Phys.* **78**, 865 (2006).
 - [23] J. Kuneš, Efficient treatment of two-particle vertices in dynamical mean-field theory, *Phys. Rev. B* **83**, 085102 (2011).
 - [24] A. Niyazi, D. Geffroy, and J. Kuneš, Antiferromagnetic magnons and local anisotropy: Dynamical mean-field study, *Phys. Rev. B* **104**, 075152 (2021).
 - [25] A. A. Mostofi, J. R. Yates, G. Pizzi, Y.-S. Lee, I. Souza, D. Vanderbilt, and N. Marzari, An updated version of wannier90: A tool for obtaining maximally-localised wannier functions, *Comput. Phys. Commun.* **185**, 2309 (2014).
 - [26] J. Kuneš, R. Arita, P. Wissgott, A. Toschi, H. Ikeda, and K. Held, Wien2wannier: From linearized augmented plane waves to maximally localized wannier functions, *Comput. Phys. Commun.* **181**, 1888 (2010).

- [27] P. Blaha, K. Schwarz, G. Madsen, D. Kvasnicka, and J. Luitz, *WIEN2k, An Augmented Plane Wave + Local Orbitals Program for Calculating Crystal Properties (Karlheinz Schwarz, Techn. Universitat Wien, Austria, 2001), ISBN 3-9501031-1-2*.
- [28] Supplemental Material.
- [29] A. Georges, G. Kotliar, W. Krauth, and M. Rozenberg, Dynamical mean-field theory of strongly correlated fermion systems and the limit of infinite dimensions, *Rev. Mod. Phys.* **68**, 13 (1996).
- [30] E. Gull, A. J. Millis, A. I. Lichtenstein, A. N. Rubtsov, M. Troyer, and P. Werner, Continuous-time Monte Carlo methods for quantum impurity models, *Rev. Mod. Phys.* **83**, 349 (2011).
- [31] P. P. Stavropoulos, X. Liu, and H.-Y. Kee, Magnetic anisotropy in spin-3/2 with heavy ligand in honeycomb Mott insulators: Application to CrI_3 , *Phys. Rev. Research* **3**, 013216 (2021).
- [32] M. Jarrell and J. Gubernatis, Bayesian inference and the analytic continuation of imaginary-time quantum Monte Carlo data, *Physics Reports* **269**, 133 (1996).
- [33] J. P. Perdew, K. Burke, and M. Ernzerhof, Generalized gradient approximation made simple, *Phys. Rev. Lett.* **77**, 3865 (1996).
- [34] X. Wang, E. Gull, L. de' Medici, M. Capone, and A. J. Millis, Antiferromagnetism and the gap of a Mott insulator: Results from analytic continuation of the self-energy, *Phys. Rev. B* **80**, 045101 (2009).
- [35] X. Liu, D. Churchill, and H.-Y. Kee, Theoretical analysis of single-ion anisotropy in d^3 Mott insulators, *Phys. Rev. B* **106**, 035122 (2022).
- [36] Y. Miura, Y. Yasui, M. Sato, N. Igawa, and K. Kakurai, New-type phase transition of Li_2RuO_3 with honeycomb structure, *Journal of the Physical Society of Japan* **76**, 033705 (2007).
- [37] G. Bastien, G. Garbarino, R. Yadav, F. J. Martinez-Casado, R. Beltrán Rodríguez, Q. Stahl, M. Kusch, S. P. Limandri, R. Ray, P. Lampen-Kelley, D. G. Mandrus, S. E. Nagler, M. Roslova, A. Isaeva, T. Doert, L. Hozoi, A. U. B. Wolter, B. Büchner, J. Geck, and J. van den Brink, Pressure-induced dimerization and valence bond crystal formation in the kitaev-heisenberg magnet $\alpha\text{-RuCl}_3$, *Phys. Rev. B* **97**, 241108 (2018).
- [38] T. Takayama, M. Blankenhorn, J. Bertinshaw, D. Haskel, N. A. Bogdanov, K. Kitagawa, A. N. Yaresko, A. Krajewska, S. Bette, G. McNally, A. S. Gibbs, Y. Matsumoto, D. P. Sari, I. Watanabe, G. Fabbri, W. Bi, T. I. Larkin, K. S. Rabinovich, A. V. Boris, H. Ishii, H. Yamaoka, T. Irifune, R. Bewley, C. J. Ridley, C. L. Bull, R. Dinnebier, B. Keimer, and H. Takagi, Competing spin-orbital singlet states in the $4d^4$ honeycomb ruthenate $\text{Ag}_3\text{LiRu}_2\text{O}_6$, *Phys. Rev. Res.* **4**, 043079 (2022).
- [39] T. Marchandier, G. Rousse, Q. Jacquet, A. M. Abakumov, F. Fauth, C. V. Colin, and J.-M. Tarascon, Magnetic and intercalation properties of BaRu_2O_6 and SrRu_2O_6 , *Chemistry of Materials* **32**, 8471 (2020).
- [40] W. Metzner and D. Vollhardt, Correlated lattice fermions in $d = \infty$ dimensions, *Phys. Rev. Lett.* **62**, 324 (1989); A. Georges and G. Kotliar, Hubbard model in infinite dimensions, *Phys. Rev. B* **45**, 6479 (1992); M. Jarrell, Hubbard model in infinite dimensions: A quantum Monte Carlo study, *Phys. Rev. Lett.* **69**, 168 (1992).
- [41] H. Shinaoka, E. Gull, and P. Werner, Continuous-time hybridization expansion quantum impurity solver for multi-orbital systems with complex hybridizations, *Computer Physics Communications* **215**, 128 (2017).
- [42] P. Werner, A. Comanac, L. de' Medici, M. Troyer, and A. J. Millis, Continuous-time solver for quantum impurity models, *Phys. Rev. Lett.* **97**, 076405 (2006).
- [43] A. Gaenko, A. E. Antipov, G. Carcassi, T. Chen, X. Chen, Q. Dong, L. Gamper, J. Gukelberger, R. Igarashi, S. Iskakov, M. Könz, J. P. LeBlanc, R. Levy, P. N. Ma, J. E. Paki, H. Shinaoka, S. Todo, M. Troyer, and E. Gull, Updated core libraries of the ALPS project, *Comput. Phys. Commun.* **213**, 235 (2017); B. Bauer, L. D. Carr, H. G. Evertz, A. Feiguin, J. Freire, S. Fuchs, L. Gamper, J. Gukelberger, E. Gull, S. Guertler, A. Hehn, R. Igarashi, S. V. Isakov, D. Koop, P. N. Ma, P. Mates, H. Matsuo, O. Parcollet, G. Pawłowski, J. D. Picon, L. Pollet, E. Santos, V. W. Scarola, U. Schollwöck, C. Silva, B. Surer, S. Todo, S. Trebst, M. Troyer, M. L. Wall, P. Werner, and S. Wessel, The ALPS project release 2.0: Open source software for strongly correlated systems, *J. Stat. Mech. Theory Exp.* **2011**, P05001 (2011).
- [44] H. Shinaoka, J. Otsuki, M. Kawamura, N. Takemori, and K. Yoshimi, DCore: Integrated DMFT software for correlated electrons, *SciPost Phys.* **10**, 117 (2021).
- [45] V. Zlatić and B. Horvatic, *Solid State Commun.* **75**, 263 (1990).
- [46] L. Boehnke, H. Hafermann, M. Ferrero, F. Lechermann, and O. Parcollet, Orthogonal polynomial representation of imaginary-time green's functions, *Phys. Rev. B* **84**, 075145 (2011).
- [47] D. Geffroy, J. Kaufmann, A. Hariki, P. Gunacker, A. Hausoel, and J. Kuneš, Collective modes in excitonic magnets: Dynamical mean-field study, *Phys. Rev. Lett.* **122**, 127601 (2019).
- [48] R. Levy, J. LeBlanc, and E. Gull, Implementation of the maximum entropy method for analytic continuation, *Computer Physics Communications* **215**, 149 (2017).
- [49] A. Hariki, M. Winder, T. Uozumi, and J. Kuneš, LDA + DMFT approach to resonant inelastic x-ray scattering in correlated materials, *Phys. Rev. B* **101**, 115130 (2020).
- [50] M. W. Haverkort, Theory of resonant inelastic x-ray scattering by collective magnetic excitations, *Phys. Rev. Lett.* **105**, 167404 (2010).
- [51] A. Nag, H. C. Robarts, F. Wenzel, J. Li, H. Elnaggar, R.-P. Wang, A. C. Walters, M. García-Fernández, F. M. F. de Groot, M. W. Haverkort, and K.-J. Zhou, Many-body physics of single and double spin-flip excitations in NiO , *Phys. Rev. Lett.* **124**, 067202 (2020).
- [52] J. Li, Y. Gu, Y. Takahashi, K. Higashi, T. Kim, Y. Cheng, F. Yang, J. Kuneš, J. Pellicciari, A. Hariki, and V. Bisogni, Single- and multimagnon dynamics in antiferromagnetic $\alpha\text{-Fe}_2\text{O}_3$ thin films, *Phys. Rev. X* **13**, 011012 (2023).
- [53] The spin quantization axis is pointing out of plane.
- [54] As discussed in Ref. 19 SrRu_2O_6 is essentially a 2D material with T_N determined by the spin gap. The dimensionality aspect is not properly captured by DMFT.
- [55] Note that calculations in Ref. 18 put T^* to around 800 K.
- [56] R. J. Green, M. W. Haverkort, and G. A. Sawatzky, Bond disproportionation and dynamical charge fluctuations in the perovskite rare-earth nickelates, *Phys. Rev. B* **94**, 195127 (2016); Y. Lu, D. Betto, K. Fürsich, H. Suzuki, H.-H. Kim, G. Cristiani, G. Logvenov, N. B. Brookes, E. Benckiser, M. W. Haverkort, G. Khaliullin, M. Le Tacon, M. Minola, and B. Keimer, Site-selective

probe of magnetic excitations in rare-earth nickelates using resonant inelastic x-ray scattering, Phys. Rev. X **8**, 031014 (2018); M. Winder, A. Hariki, and J. Kuneš, X-ray spectroscopy of the rare-earth nickelate LuNiO_3 :

LDA + DMFT study, Phys. Rev. B **102**, 085155 (2020).
[57] S. Doniach, The Kondo lattice and weak antiferromagnetism, Physica B+C **91**, 231 (1977).